J Mater Sci (2009) 44:5475–5484
DOI 10.1007/s10853-009-3762-7

Effect of hot compression and annealing on microstructure evolution of ZK60 magnesium alloys

Shouren Wang · Suk Bong Kang · JaeHyung Cho

Received: 8 March 2009 / Accepted: 18 July 2009 / Published online: 5 August 2009

Abstract Microstructural evolution of ZK60 magnesium alloys, during twin roll cast (TRC) and hot compression (HC) with a strain rate of 0.1 s^{-1} at 350 °C and subsequent annealing at temperatures of 250–400 °C for 10^2–5×10^5 s, has been observed by optical microscopy (OM), transmission electron microscopy (TEM) and electron backscatter diffraction (EBSD). The distribution of average grain size and recrystallized grain size at different annealing conditions were calculated. Activation energy and recrystallized volume fractions during annealing were discussed using analysis of static recrystallization (SRX) kinetics. Based on examination of microstructure evolution during annealing, it was found that several SRX mechanisms were co-activated. Subgrains with high misorientation angles to surrounding grains were formed by dislocation rearrangement, and they seemed to evolve into newly recrystallized grains.

Introduction

Wrought magnesium alloys have attracted large attentions in recent years due to more advantageous mechanical properties than cast magnesium alloys [1–4]. A wide application of wrought magnesium alloys, however, is still limited because of poor formability of hexagonal close packed (hcp) materials. The number of slip systems of the hcp materials is restricted, and this results in tight formability. Basal slip usually operates at room temperature and other non-basal slip systems such as prismatic and pyramid slips start to operate at elevated temperatures. Activation energy of slip systems varies with temperature in hcp materials. Twinning also plays an important role during deformation.

To improve formability of magnesium alloys, several thermo-mechanical processing, such as twin-roll strip casting (TRC), warm rolling (WR), hot extrusion (HE), torsion straining (TS), reciprocal extrusion (RE) or equal channel angular extrusion (ECAE), were suggested. These processes combined with subsequent annealing give rise to grain refinement, fine and homogeneous distribution of 2nd particle and texture and microstructure modification. For example, the TRC process, which is skipping several thermo-mechanical steps and thus saving production cost, has a number of advantages over conventional direct chill casting (DC). The TRC process has continued to develop since it was first conceived by Henry Bessemer in 1856 [5]. During TRC, molten metals are directly converted into coiled strips which are suitable for subsequent rolling or drawing processes. Microstructure of grain size and 2nd particles heavily depends on extent of cooling rate and concurrent hot deformation during TRC.

Grain refinement is a useful strengthening mechanism to enhance both strength and elongation of materials. The strengthening mechanism is based on the fact that fine-grained materials have a larger number of grain boundaries impeding dislocation motion [6–8]. For wrought magnesium alloys, grain refinement or prevention of grain coarsening is also important to improve formability [9, 10]. Magnesium sheets fabricated by TRC have finer grains and better mechanical properties than those by DC [11].

S. Wang (✉)
School of Mechanical Engineering, University of Jinan,
Jinan 250022, China
e-mail: sherman0158@tom.com

S. Wang · S. B. Kang · J. Cho
Korea Institute of Materials Science, 66 Sangnam-dong,
Changwon 641010, South Korea
e-mail: sbkang@kims.re.kr

Stacking fault energy (SFE) can affect microstructure evolution during both deformation and annealing. In alloys of high SFE, extended dislocation width is small, and thus cross-slip easily occurs, the dynamic recovery is the main or exclusive softening mechanism. In alloys of low SFE, occurrence of cross-slip is difficult, dislocation density increases during deformation, dynamic recrystallization (DRX) or static recrystallization (SRX) occur more easily.

In order to obtain more improved mechanical properties, combined thermo-mechanical processing is effective. In this work, twin roll cast (TRC) and subsequent hot compression (HC) were used to enhance mechanical properties of ZK60 alloys. Alloys with large deformation at low temperatures usually have a high stored energy and a large fraction of non-equilibrium grain boundaries, and thus reveal a lower thermal stability [12, 13]. This results in failure during forming process. For further usage of TRC-HCed ZK60 alloys, annealing processes were carried out. Annealing releases stored energy and restores the ductility of deformed materials. A comprehensive understanding of annealing mechanisms after severe plastic deformation has not been obtained yet due to scarcity of systematic experimental data [14]. DRX and SRX are not fully understood either. The present work focused on microstructural evolution of ZK60 magnesium alloys during deformation and subsequent annealing. Mechanisms of recrystallization were discussed based on the microstructure evolution.

Experimental procedure

Materials used in the present work were commercial magnesium alloys, ZK60. Chemical compositions of the alloys were Mg–6.20%Zn–0.48%Zr in weight percent. Detailed TRC processing is shown in the literature [15]. Schematic diagrams of combined TRC-HC processing are shown in Fig. 1. Uniaxial hot compression tests (HC) were performed at a temperature of 350 °C and strain rate of 0.1 s^{-1}. Hot compressed specimens were quenched using nitrogen gas immediately after compression in order to prevent microstructural changes. The samples were annealed at different temperatures (250, 300, 350, and 400 °C) and times (100, 1000, 5000, 10000, and 50000 s). Annealed samples were mechanically polished with polycrystalline diamond suspension of glycol-based solution. Grain structure was revealed by subsequent etching in 7 s with a solution of picric acid (5 g), acetic acid (5 mL), distilled water (10 mL), and ethanol (100 mL). All optical micrographs (OM) were taken along the transverse direction of rolling sheets. The average grain size of ZK60 alloys was analyzed by an image analyzer. HV hardness values were measured by digital microhardness tester (TOKYO, MXT70). Pole figures were obtained using electron backscatter diffraction (EBSD). Precipitates and sub-grains were observed using a JEM-2100F transmission electron microscope (TEM) operating at 200 kV. Thin foils parallel to the rolling direction were prepared by a twin jet electro-

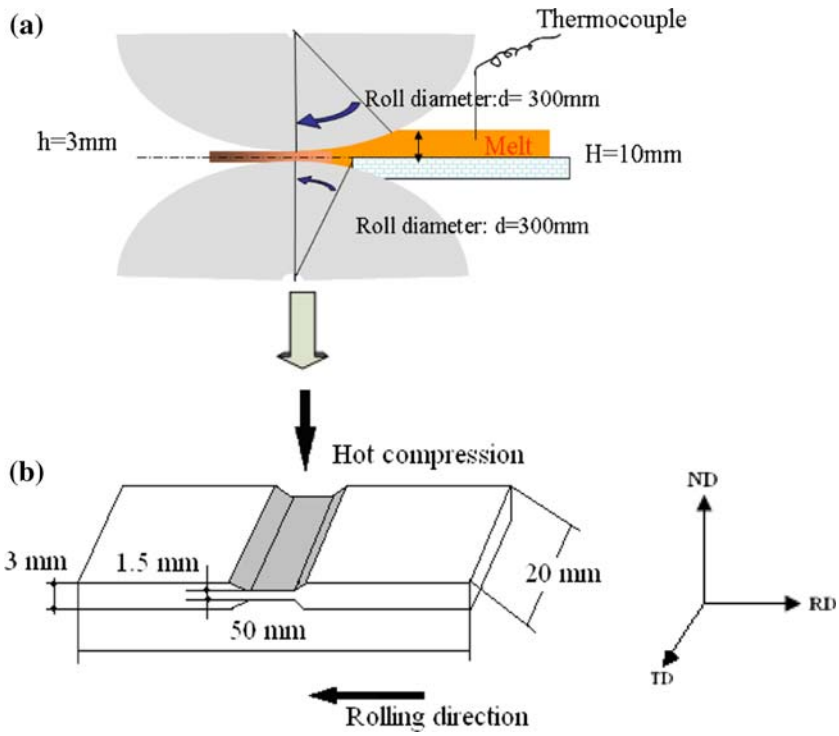

Fig. 1 Schematic diagrams of the TRC-HC processing: **a** TRC and **b** HC

polisher using a solution of $HClO_4$ (5%), butanol (35%) and methanol (60%), and then ion-beam milled.

Results

Microstructure comparisons of ZK60 alloys between TRC and combined TRC-HC processing are shown in Fig. 2. There exist distinct structural variations in microstructure of TRC samples compared with conventional DC samples. Coarser and equiaxed grains are usually observed in the DC samples. Some second eutectics and intermetallic compounds are also distributed along the grain boundaries or the interior of grains [16, 17]. In a TRC state, it is difficult to find equiaxed grains. From Fig. 2a, it is shown that there exists a dendrite structure, and some particles are embedded in the interdendritic region. The size of particles is much finer than that in DC samples. Compared with DC, TRC processing possesses numerous advantages of not only microstructure modification (less segregation, uniform distribution of grain size, grain refinement, and so on) but also mechanical properties. Microstructure evolution of the combined TRC-HCed Mg alloys is different from that of TRC or DC samples. In Fig. 2b, there exist many deformation or shear bands in the microstructure of TRC-HCed alloys. Recrystallized small grains were found along the initial grain boundaries (inset of Fig. 2b). Some twins are also observed inside grains (an arrow in inset of Fig. 2b). Overall, it can be seen that there are distinct bimodal structures consisting of a large fraction of the original and deformed grains with a small fraction of newly developed grains.

Figure 3 displays microstructural evolution of ZK60 alloys during both hot compression and annealing. Hot compression was made at 350 °C with a strain rate of 0.1 s^{-1}, and total strain of 0.5, and subsequent annealing at various temperatures (250, 300, 350, and 400 °C) and times (100, 1000, 5000, and 10000 s). At an annealing temperature of 250 °C, there were no distinct structural changes depending on the annealing time (Fig. 3a–d). Instead, large deformed grains were clearly distinguishable from surrounding fine grains. Some subgrain boundaries began to migrate driven by thermal energy and evolved into newly recrystallized grains. This process started in the beginning of annealing process and finished in a short time. In general, short annealing times at low temperatures were not enough to complete sufficient static recrystallization (SRX). Twin structure is still observed in Fig. 3b and f because of insufficient annealing time and low temperature for full recrystallization. When 250 °C $< T <$ 300 °C, grain growth looks clearer with increase in annealing time. When annealed at 300 °C for 1000 s, recrystallized fine grains were found along the shear bands (see Fig. 3f). Their average grain size is about 3.2 μm. Most twins were eliminated once annealing time exceeded 5000 s, indicating completion of recrystallization. It is different from conclusions of other literature on AZ31B, which reported recrystallization completed in a short time [18]. When annealing time was extended up to 10000 s, ZK60 alloys were fully-recrystallized, and fine and nearly uniform equiaxed grains were obtained (as shown in Fig. 3h). It is indicated that SRX has been nearly finished and grain growth has begun. When 300 °C $< T <$ 350 °C, initial grains began to grow quickly in the beginning of annealing

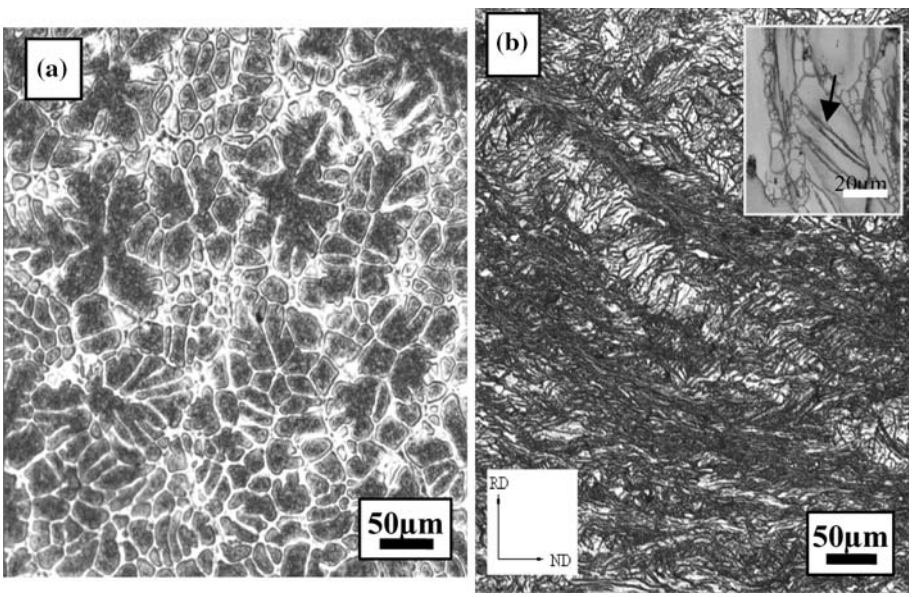

Fig. 2 Microstructure comparison of ZK60 alloys at **a** TRC and **b** TRC-HC

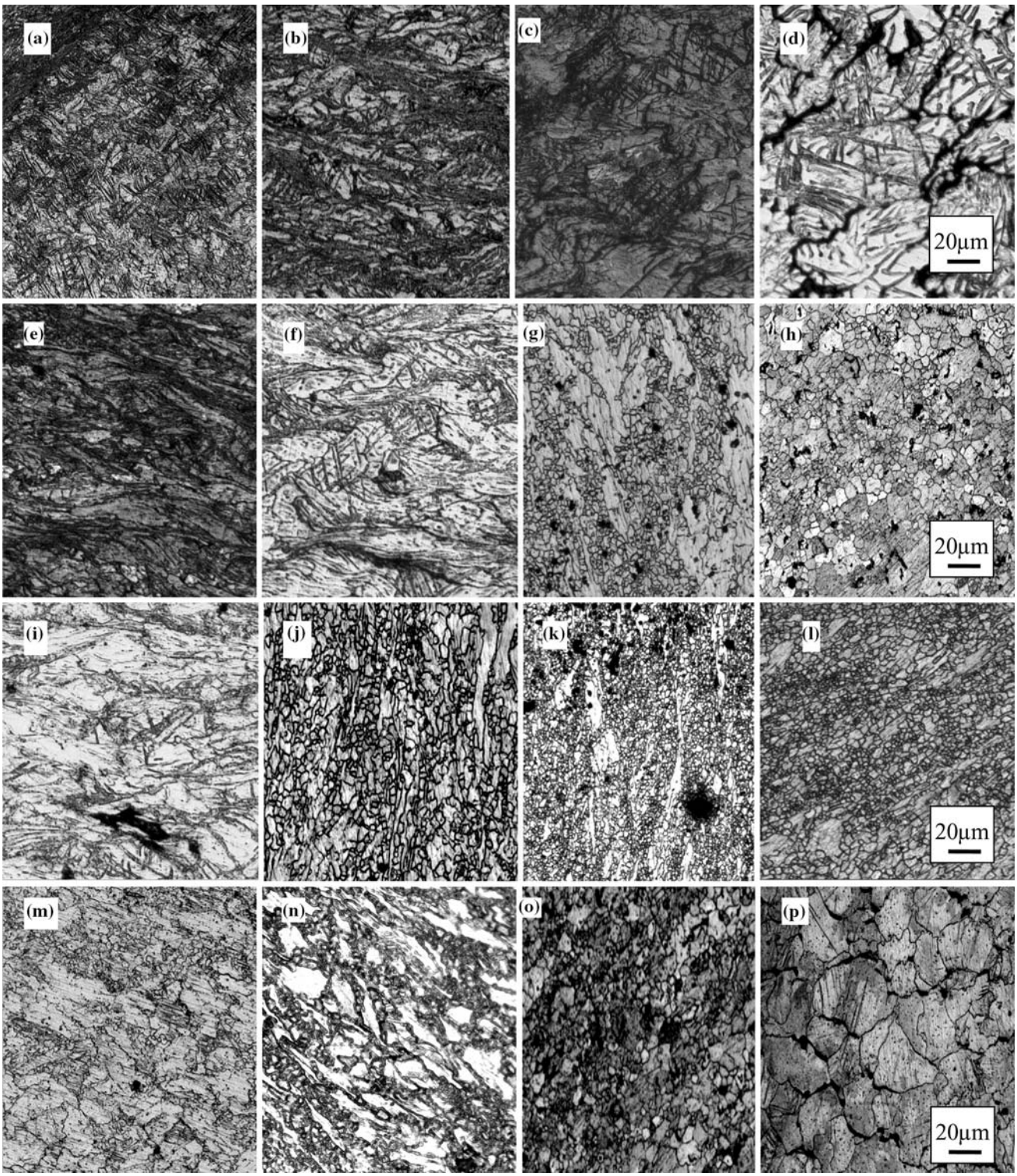

Fig. 3 Microstructural evolution of ZK60 alloys during both hot compression and subsequent annealing. HC processes were carried out at a temperature of 350 °C, a strain rate of 0.1 s^{-1}, and a total strain of 0.5. Subsequent annealing was made at different temperatures and times of 250 °C for **a** 100 s, **b** 1000 s, **c** 5000 s, and **d** 10000 s; 300 °C for **e** 100 s, **f** 1000 s, **g** 5000 s, and **h** 10000 s; 350 °C for **i** 100 s, **j** 1000 s, **k** 5000 s, and **l** 10000 s; 400 °C for **m** 100 s, **n** 1000 s, **o** 5000 s, and **p** 10000 s

and became bigger with increase in annealing time. SRX nearly finished after 1000 s at 350 °C, and only a few deformed grains were observed (shown in Fig. 3j). The average grain size of them is 6.9 μm. When annealing temperature increased up to 400 °C, recrystallization was easy to begin and complete. SRX was nearly finished after

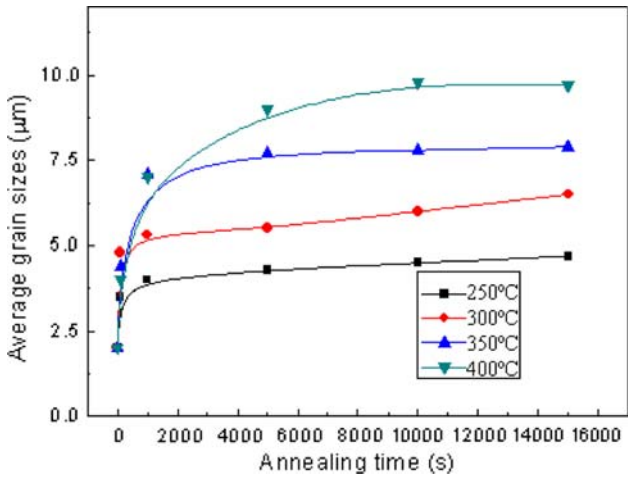

Fig. 4 Average grain sizes of ZK60 alloys during annealing at different temperatures and times

100 s at 400 °C, and a few large grains were found (see Fig. 3m). Those large grains looked like rather continuous recrystallization or extended recovery than conventional recrystallization. Fully recrystallized grains were obtained after 1000 s (Fig. 3n). At the same time, new grains began to grow and became coarser (see Fig. 3o). The average grain size is 8.4 μm. In Fig. 3p, the newly recrystallized grains were finally developed, and the grains by continuous recrystallization or extended recovery were eliminated. Continuous increase in annealing time resulted in grain growth after recrystallization. Usually, grains by continuous recrystallization (or extended recovery) still have higher stored energy. They were eaten by newly recrystallized grains after enough annealing time. Figure 4 displays variation of average grain sizes with annealing time and temperature. It is shown that the average grain size increases as the annealing temperature increases. At a specified temperature, grain size quickly increased at the beginning of annealing, and it revealed that microstructure started to fast evolve. These trends look clearer during annealing at higher temperatures than at lower temperatures.

Discussion

Static recrystallization kinetics

It is well known that some processing parameters (strain rate, total strain and temperature during deformation, and time and temperature during annealing and so on) and structural features (textures, grain topology and 2nd particles and so on) have primary effects on SRX [19]. The kinetics of SRX is usually described by JMAK model (Johnson, Mehl, Avrami and Kolmogorov). If stored energy is homogeneous and nuclei are randomly distributed, the theoretical model can be widely used for the description of recrystallization kinetics [19, 20]:

$$X(t) = 1 - \exp(-bt^m), \tag{1}$$

where $X(t)$ is the recrystallized volume fraction during annealing and t is annealing time. A constant, b, depends on nucleation and growth, and m is an Avrami exponent. If stored energy is non-homogeneous, and nuclei are formed heterogeneously, then Eq. 1 is invalid.

The recrystallized volume fraction, $X(t)$, obtained at various annealing times and temperatures produced sigmoidal-shaped curves for ZK60 alloys, as shown in Fig. 5. The JMAK equation (Eq. 1) in logarithms can be rewritten as

$$\ln\left(\ln\frac{1}{1-X(t)}\right) = \ln b + m\ln t. \tag{2}$$

Variations of recrystallized volume fractions with annealing time were analyzed at various temperatures in Fig. 5. Using a linear regression method, m and b values in Eq. 2 were determined. The slope of $\ln(\ln[1/(1-X(t))])$ versus $\ln t$ yielded m and b at various annealing temperatures (Fig. 6). SRX usually starts quickly and finishes slowly, and thus a more useful form of JMAK equation based on the time required to obtain 50% recrystallization ($t_{0.5}$) can be used alternatively

$$X(t_{0.5}) = 1 - \exp\left(-bt_{0.5}^m\right). \tag{3}$$

The calculated and measured parameters of ZK60 alloys are summarized in Table 1. It is noted that $t_{0.5}$ varies largely with increase in temperature (T). The higher the temperature is, the shorter $t_{0.5}$ is. The value of m is nearly equivalent ($m = 2.25$), while b is easily varied with temperature b

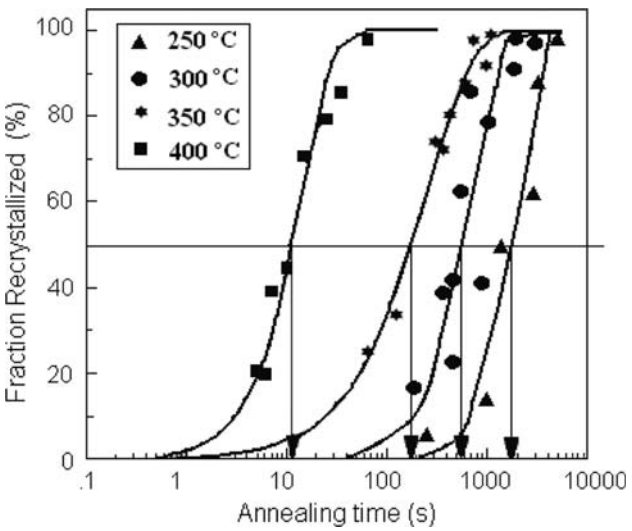

Fig. 5 Variations of recrystallized volume fractions with annealing time at various temperatures

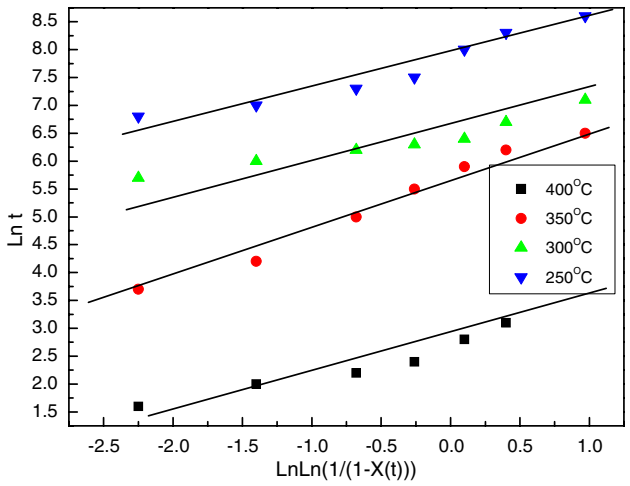

Fig. 6 Linear regression between ln(t) and ln(ln[1/(1 − $X(t)$)]) at different temperatures

Table 1 Calculated and measured parameters of ZK60 alloys

T (°C)	$t_{0.5}$ (s)	m	b
250	4600	2.25	7.87×10^{-7}
300	720	2.25	5.45×10^{-5}
350	200	2.25	3.53×10^{-3}
400	15	2.25	1.51×10^{-1}

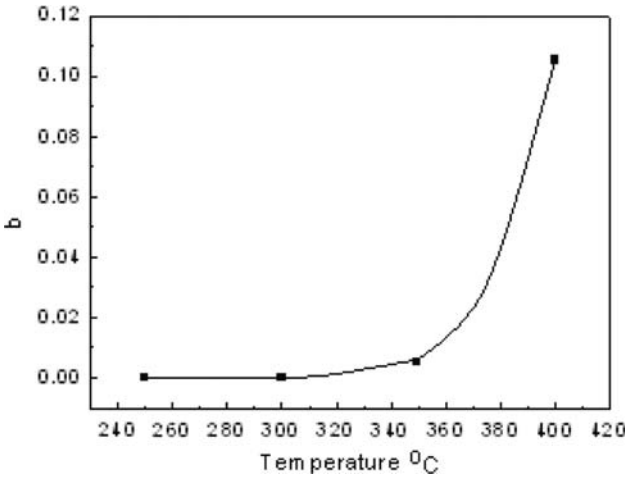

Fig. 7 Relationship between b and temperature (T)

ranging from 1.51×10^{-1} to 7.87×10^{-7}, according to temperatures of 250 to 400 °C, respectively. The relationship between b and T is shown in Fig. 7, which shows a sharp increase of b with increase in T.

The activation energy for grain growth was calculated to elucidate grain growth mechanisms during static annealing. As an approximation, the growth of grains in the temperature range of interest is assumed to follow the general equation of grain growth,

$$d^{n'} - d_0^{n'} = kt, \tag{4}$$

where d is the grain size at a given annealing time, d_0 is the initial grain size, and t is the annealing time. Equation 4 is known as the Burke and Turnbull's equation, and the constant, n', is often termed as a grain growth exponent, given by 2, so,

$$d^2 - d_0^2 = kt. \tag{5}$$

k is a temperature-dependent constant that can be described by Arrhenius equation

$$k = k_0 \exp\left(-\frac{Q}{RT}\right), \tag{6}$$

where k_0 is the constant, Q is the activation energy for grain growth and R is the gas constant. From this Arrhenius equation, it is indicated that k is related to the speed of recrystallization (high temperature and low activation energy can accelerate SRX), while recrystallized speed is inversely proportional to annealing time (t), so k is inversely proportional to t,

$$\frac{1}{t} = A' \exp\left(-\frac{Q}{RT}\right), \tag{7}$$

$$\frac{t_1}{t_2} = \exp\left[-\frac{Q}{R}\left(\frac{1}{T_2} - \frac{1}{T_1}\right)\right]. \tag{8}$$

Based on Eq. 8 and Table 1, Q values depending on temperatures of 250–300 °C, 300–350 °C and 350–400 °C can be calculated as 89.6, 78.8 and 172.2 kJ/mol, respectively.

Mechanisms of microstructural evolution during annealing

Figure 8 shows results of X-ray diffraction (XRD) of ZK60 alloys at (a) various annealing temperatures and (b) annealing times. Several important crystal planes, (0002), $(10\bar{1}0)$, $(10\bar{1}1)$, $(10\bar{1}2)$ and $(10\bar{1}3)$ are marked. It was shown that with increase in annealing temperature, intensities of basal planes were gradually weakened, while intensities of non-basal planes such as $(10\bar{1}0)$ and $(10\bar{1}1)$ gradually increased (Fig. 8a). For example, non-basal peaks of $(10\bar{1}0)$ and $(10\bar{1}1)$ grew stronger during annealing for 1000 s at 400 °C. Note that intensity of the $(10\bar{1}1)$ plane nearly disappeared under annealing conditions of 350 °C for 50000 s. Dislocation rearrangement during hot deformation can play an important role in formation of substructures or embryos for recrystallization (arrow in Fig. 9a), and thus texture intensities can vary with temperature during subsequent static recrystallization (arrows in Fig. 9b). This was consistent with conclusions of other

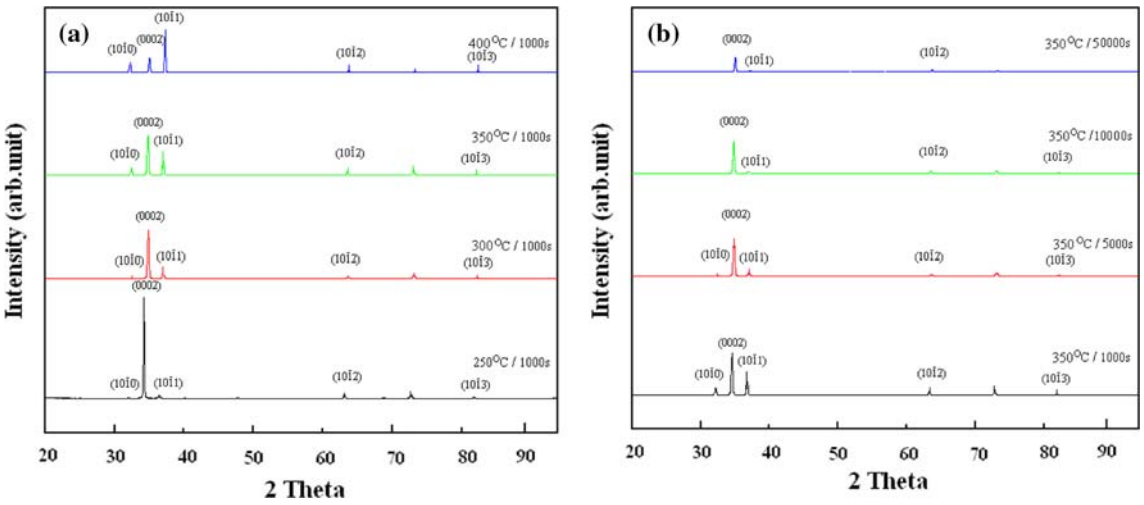

Fig. 8 Results of X-ray diffraction of ZK60 alloys at **a** different annealing temperatures and **b** different annealing times

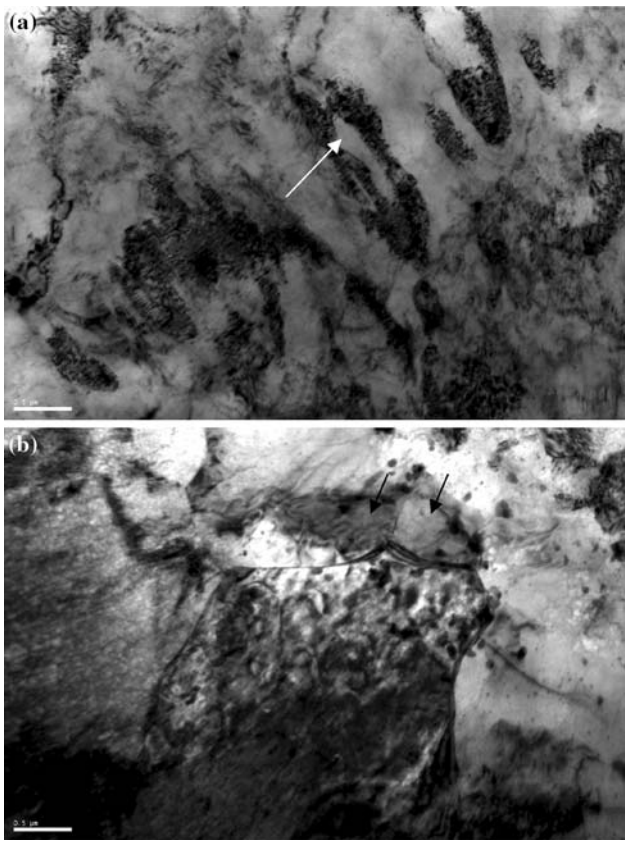

Fig. 9 TEM micrographs after **a** deformation and **b** subsequent annealing at 350 °C for 1000 s

literatures [21, 22]. To investigate texture evolution during annealing, EBSD measurements were carried out along the normal direction (ND). As-deformed samples possessed a strong basal texture, which causes the *c*-axis aligned in the ND as shown in Fig. 10a. Annealing at 400 °C for 1000 s caused changes in both basal and non-basal textures (Fig. 10b). In particular, the intensity of the basal planes decreased a lot, compared to that of the as-deformed.

Variations in annealing time also result in the change of intensities of crystallographic planes (Fig. 8b). With increase in annealing time, both basal and non-basal peaks were weakened. In particular, non-basal peaks of $(10\bar{1}0)$ and basal, (0002) revealed a significant reorientation or weakening. During annealing at 350 °C more than 1000 s, recrystallization is almost finished and grain growth is dominant as shown in Fig. 5. Grain growth is mainly controlled by grain boundary motion, which can be affected by the changes in solutes and precipitates in ZK60 alloys during annealing. Variations of precipitates during annealing process were investigated by TEM micrographs shown in Fig. 11. It is clear that a great number of particles distinctly decrease with increase in annealing time. The change in precipitates can affect grain growth and texture evolution during annealing.

Despite numerous literatures on microstructural evolution of deformed materials during annealing [23–25], mechanisms of SRX are not yet fully understood due to the complexities of the phenomenon, i.e. formation of subgrain embryo and subgrain boundary migration. Subgrains with a high misorientation angle to adjacent grains frequently have enough mobility to evolve into newly recrystallized grains [26]. A high-angle sub-boundary can be formed through progressive lattice misorientation between subgrains. The disorientation angle, θ, is related to the spacing, (h), of dislocations in a sub-boundary and length of the Burgers vector (b). Considering a tilt boundary, θ, is described as,

$$\theta = 2\tan\left(\frac{\theta}{2}\right) = \frac{b}{h}. \tag{9}$$

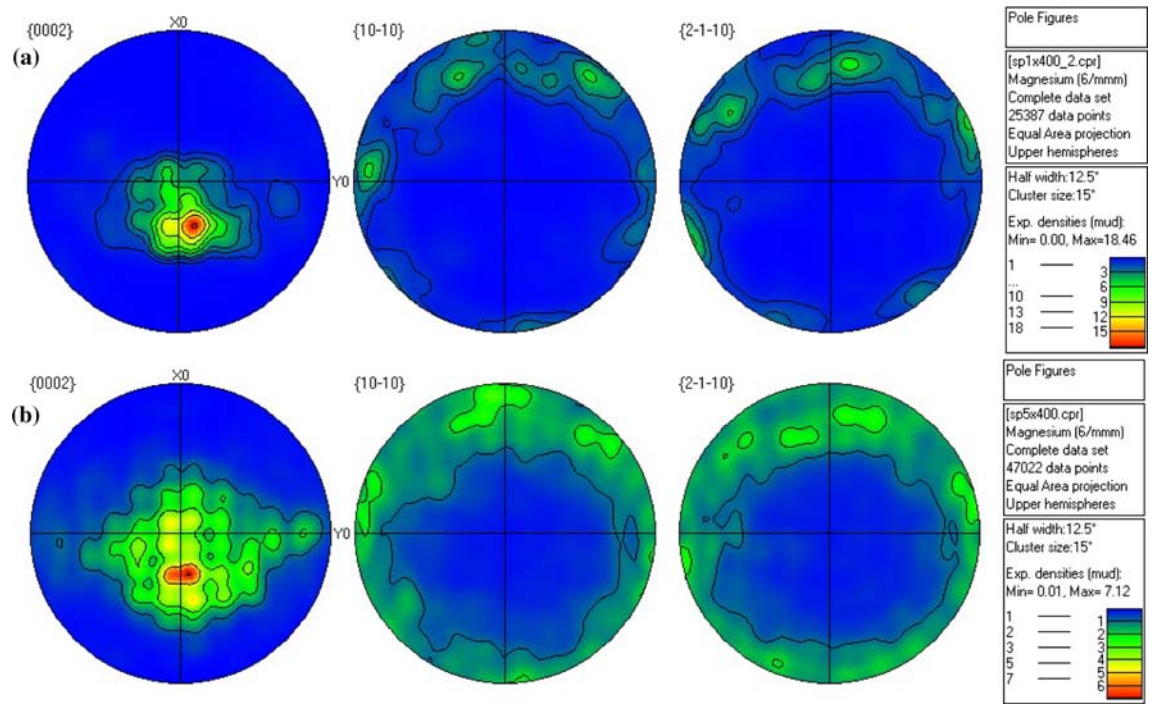

Fig. 10 Pole figures of ZK60 alloys deformed at 350 °C with a strain rate of 0.1 s^{-1}. **a** As-deformed and **b** annealing at 400 °C for 1000 s

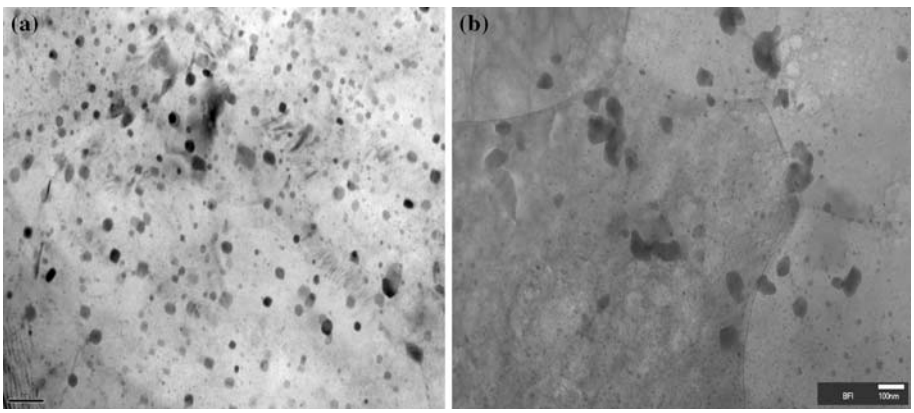

Fig. 11 Precipitate comparison using TEM micrographs in different annealing conditions of **a** 350 °C for 1000 s and **b** 350 °C for 10000 s

The critical angle, θ_C, is given as 10–15°. If $\theta < \theta_C$, it is regarded as low-angle boundaries, if $\theta > \theta_C$, it is regarded as high-angle boundaries. It is indicated that some specific high-angle grain boundaries could be identified to have significantly higher mobility than other grain boundaries. The high-angle sub-boundaries are driven by dislocation climb and glide, and then begin to rotate. The rotated sub-boundaries change into high-angle boundaries and consume neighboring subgrains.

Nucleation of recrystallization usually occurs in the various sites with high local misorientations, such as: (i) pre-existing high-angle grain boundaries; (ii) transition bands; (iii) shear bands; and (iv) regions near large or hard particles [26, 27]. Therefore, there are various mechanisms of microstructural evolution, such as grain boundary migration (GBM), grain boundary bulging (GBB), subgrain rotation (SGR). A combination of the evolution mechanisms of deformed metals during annealing are conjectured to be co-activated. The optical micrographs of ZK60 alloys during deformation with a temperature of 350 °C and a strain rate, 0.1 s^{-1}, and during subsequent annealing at 350 °C for 1000 s are shown in Fig. 12. Grain boundary protrusions are observed in Fig. 12a (arrows), illustrating that some grain boundaries migrate by boundary protrusions, and bowing out from neighbored grains. Figure 12b shows the GBB mechanism. The serrated grain boundary is distinct. Some intra-crystalline grain nucleates and grows relying on the SGR mechanism (Fig. 12c, arrows). In addition, some marginal grains (Fig. 12d, arrows) are

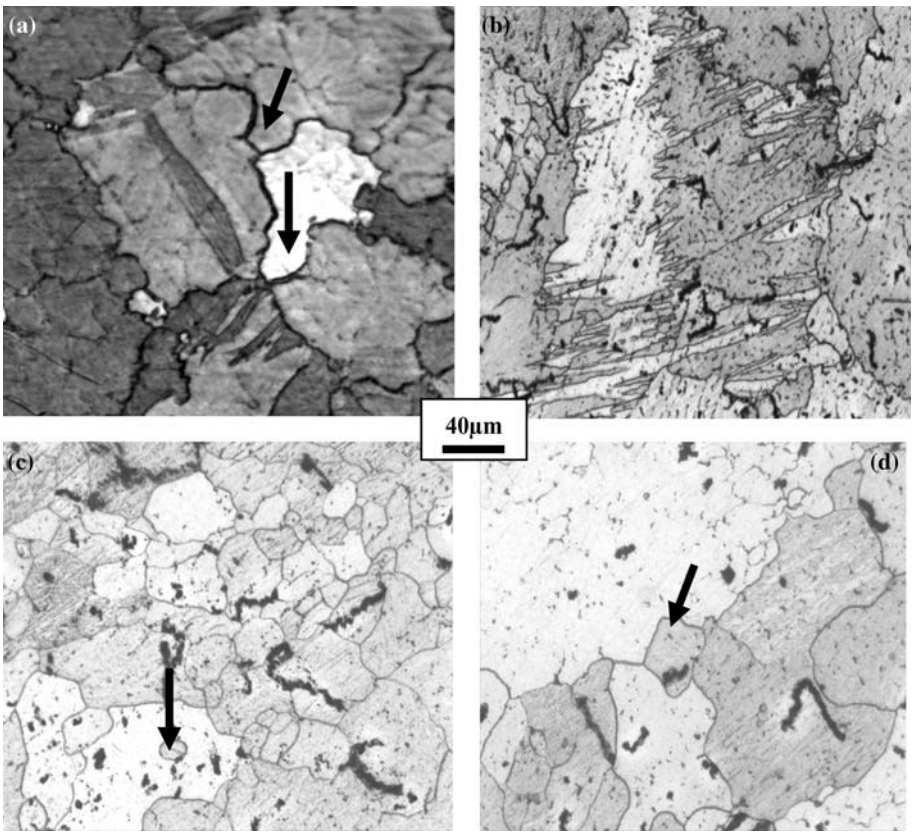

Fig. 12 Mechanisms of microstructural evolution of ZK60 alloys: **a** GBM; **b** GBB; **c** SGR of intra-crystalline grain and **d** SGR of marginal grains

likely to nucleate and grow by the SGR mechanism. DRX during deformation is to partially complete, and thus there coexist some recovery or deformation zones, where recrystallization (or SRX) continues to occur during subsequent annealing.

Conclusions

Microstructural evolution of ZK60 magnesium alloys were discussed during TRC, subsequent HC and annealing.

1. Both annealing temperature and time have primary effect on SRX. SRX is nearly finished after 10^3 s during annealing at temperatures of 300, 350 and 400 °C. Annealing at 250 °C, SRX continues to occur until 10000 s.
2. SRX mechanisms attributed to the formation of subgrain embryos and subgrain boundary migration. A combination of evolutional mechanisms of deformed metals such as GBM, GBB and SGR are usually assumed to be co-activated.
3. Dissolution of precipitates into the matrix during annealing results in variation of mobilities of grain boundaries and affects microstructure evolution and texture. Dislocation rearrangement during deformation at elevated temperature forms substructure to result in occurrence of static recrystallization during subsequent annealing.

Acknowledgements This work was supported by the KIMS-NIMS international collaboration project and the Core Technology R & D program for the development of high-performance eco-friendly structural materials which was funded by the Korean Ministry of Commerce, Industry and Energy (Project No. 10020072) and Natural Science Foundation of Shandong Province (Y2008F27). The authors thank Mr. S.S. Jung and Mr. D.B. Kim for twin roll strip casting and Mr. E.S. Woo for hot compression test, who are working in Korea Institute of Materials Science.

References

1. Song SX, Horton JA, Kim NJ, Nieh TG (2007) Scr Mater 56:393
2. Wang GY, Wang XJ, Chang H, Wu K, Zheng MY (2007) Mater Sci Eng A 464:52
3. Galiyev A, Kaibyshev R, Gottstein G (2001) Acta Mater 49:1199
4. Liu WC, Dong J, Zhang P (2009) J Mater Sci 44(11):2916. doi: 10.1007/s10853-009-3385-z
5. Watari H, Davey K, Rasgado MT, Haga T, Izaw S (2004) J Mater Process Technol 155–156:1662
6. Armstrong RW (1968) Acta Metall 16:347
7. Barnett MR, Keshavarz Z, Beer AG (2004) Acta Mater 52:5093

8. Wang Y, Zhang Y, Zeng X (2006) J Mater Sci 41(12):3603. doi: 10.1007/s10853-005-5564-x
9. Slooff FA, Zhou J, Duszczyk J (2008) J Mater Sci 43(22):7165. doi:10.1007/s10853-008-3014-2
10. Lin JB, Wang QD, Peng LM (2008) J Mater Sci 43(21):6920. doi: 10.1007/s10853-008-2994-2
11. Chen H, Kang S-B, Yu H, Kim H-W, Min G (2008) Mater Sci Eng A 492:317
12. Takayama A, Yang X, Miura H, Sakai T (2008) Mater Sci Eng A 478:221
13. Hou LF, Wei YH, Liu BS (2008) J Mater Sci 43(13):4658. doi: 10.1007/s10853-008-2668-0
14. Barnett MR, Beer AG, Atwell D, Oudin A (2004) Scr Mater 51:19
15. Bae JW, Kang CG, Kang SB (2007) J Mater Process Technol 191:251
16. Eddahbi M, del Valle JA, Perez-Prado MT, Ruano OA (2005) Mater Sci Eng A 410–411:308
17. Beer AG, Barnett MR (2008) Mater Sci Eng A 485:318
18. Jain A, Duygulu O, Brown DW (2008) Mater Sci Eng A 486:545
19. Kazeminezhad M (2008) Mater Sci Eng A 486:202
20. Rollett AD (1997) Prog Mater Sci 42:79
21. Mackenzie LWF, Pekguleryuz M (2008) Mater Sci Eng A 480: 189
22. Bonarski BJ, Schafler E, Mingler B (2008) J Mater Sci 43(23–24):7513. doi:10.1007/s10853-008-2794-8
23. Chun YB, Hwang SK (2008) Acta Mater 56:369
24. Humphreys FJ, Hatherly M (2004) Recrystallization and related annealing phenomena. Elsevier, Oxford, p 259
25. Lin L, Chen LJ, Liu Z (2008) J Mater Sci 43(13):4493. doi: 10.1007/s10853-008-2650-x
26. Doherty RD, Hughes DA, Humphreys FJ, Jonas JJ, Juul Jensen D, Kassner ME, King WE, McNelley TR, McQueen HJ, Rollett AD (1997) Mater Sci Eng A 238:219
27. Hakamada M, Watazu A, Saito N (2008) J Mater Sci 43(6):2066. doi:10.1007/s10853-008-2474-8